




# Voltage and Current Reference Based MPPT Under Rapidly Changing Irradiance and Load Resistance

Vibhu Jatelly , Somesh Bhattacharya , *Member, IEEE*, Brian Azzopardi , *Senior Member, IEEE*, Antoine Montgareuil, Jyoti Joshi, and Sudha Arora, *Member, IEEE*

**Abstract**—This paper formulates a maximum power point tracking (MPPT) technique that accurately tracks the maximum power point of photovoltaic (PV), which undergoes simultaneous or independent sudden changes in load resistance and irradiance. The proposed algorithm is fundamentally divided into three parts; current and voltage perturbation algorithm (IPA/VPA), perturbation step-size reduction algorithm (PSSRA) and a deviation avoidance loop. The use of dual perturbation parameters using IPA and VPA ensures high tracking speed. PSSRA iteratively reduces the perturbation step-size of IPA and VPA and helps in reducing the power oscillations around MPP. Finally, a deviation avoidance loop is developed to detect a change in irradiance by examining the sign of the slope of the two power curves, namely P-V and P-I. The algorithm compares the per unit change in voltage and current of PV, to determine a simultaneous change in both irradiance and load resistance. The proposed algorithm is compared with two recently developed MPPT algorithms. The results show that the proposed technique can track the MPP with high speed and low steady-state oscillations and does not deviate from the MPP tracking path regardless of fast changes in irradiance and load resistance.

**Index Terms**—Current perturbation, voltage perturbation, boost converter, MPPT, perturb and observe.

## I. INTRODUCTION

WITH the large scale disposal of PVs for various categories starting from home applications to satellite technologies, the output efficiency of the PVs have an essential role to play. The philosophy of maximum power point tracking (MPPT) for PVs help in achieving the goal of injecting the maximum available power to the system of interest.

Among the existing MPPT techniques, hill climbing based P&O technique is most widely used due to its ease of implementation. The performance of P&O algorithm depends on

Manuscript received July 23, 2020; revised November 14, 2020; accepted February 4, 2021. Date of publication February 10, 2021; date of current version August 20, 2021. This work was supported in part by the European Commission H2020 Twinning JUMP2Excel project under Grant 810809. Paper no. TEC-00745-2020. (*Corresponding author: Vibhu Jatelly.*)

Vibhu Jatelly, Somesh Bhattacharya, and Brian Azzopardi are with the MCAST Energy Research Group, MCAST, Paola PLA9032, Malta (e-mail: vibhujatelly@gmail.com; somesh.bhattacharya0212@gmail.com; brian.azzopardi@ieec.org).

Antoine Montgareuil is with the CEA, Cadarache, 13115 Saint-Paul-lez-Durance, France (e-mail: gdm@cea.fr).

Jyoti Joshi and Sudha Arora are with the Department of Electrical Engineering, College of Technology, G. B. Pant University of Agriculture and Technology, Pantnagar 263145, India (e-mail: jyjotij25@gmail.com; arora.sudha@gmail.com).

Color versions of one or more figures in this article are available at <https://doi.org/10.1109/TEC.2021.3058454>.

Digital Object Identifier 10.1109/TEC.2021.3058454

carefully choosing the perturbation step-size [1]. The use of a large step-size result in a high speed of tracking but with a penalty of large steady-state power oscillations. On the other hand, a small step-size reduces the power oscillations, but it also slows down the tracking process. Adaptive step-size based MPPT algorithm tries to balance this trade-off between low steady-state oscillations and high tracking speed [2].

In [3], [4], the authors used a scaling parameter to adaptively change the perturbation step-size to improve the tracking speed and limit the power oscillations around MPP. The perturbation step-size is increased when the operating point is far away from MPP to speed up the tracking process, whereas the step-size is decreased when operating point is near MPP to limit the steady state oscillations. The performance of these algorithms depends on the irradiance level as it is challenging to determine a fixed value for the scaling parameter for both low and high irradiance level. In [5], the authors proposed a voltage-based P&O algorithm by carefully designing a PI controller to create an optimum voltage step. Updating the controller parameters for an optimum step-size for a large variation in irradiance is, however, challenging. In [6], the algorithm shifts the operating point to LHS of the power curve, each time it crosses over the MPP. To limit the power oscillations the algorithm uses a multiplication parameter everytime the operating point cross the MPP. However, it is difficult to determine an optimum value of this parameter under low irradiance levels. In [7], the authors proposed a Binary search (BNS) based algorithm of high tracking speed by taking a window of lower and upper bounds in voltage. The iterative reduction in the window size to half of the previous search window helps in reducing the number of iterations. But, this algorithm resets the bounds of the window to their starting values everytime there is a change in irradiance. In [8], a lock-on mechanism is suggested which iteratively reduces the perturbation step-size by using a scaling factor. The algorithm employs maximum value of this factor to iteratively reduce power oscillations. However, the use of maximum value of this scaling factor can affect the performance of the algorithm under low irradiance levels. In [9], the authors proposed a segmentation search method which reverses the tracking and multiplies the previous step-size by a constant to determine the new step-size everytime the operating point crosses the MPP. However, to determine the optimal value of this constant extensive simulations are required. In [10], the authors proposed a low-cost InC (LCInC) algorithm by eliminating the use of division computations to reduce its processing time. The algorithm uses a variable perturbation step-size,

which is evaluated by measuring the variation in power and a scaling parameter tuned during the design stage. Although, the algorithm provides low steady state oscillations as well as quick tracking capability and does not deviate from tracking path for a step change in irradiance, the tuning of this scaling parameter is challenging. In [11], the authors proposed an adaptive approach based on fractional short-circuit current ( $I_{SC}$ ) measurement by measuring  $I_{SC}$  off-line which helps in quick convergence at the MPP, but results in power losses. In [12], an adaptive perturbation frequency-based MPPT approach is suggested. This approach develops a relation between the perturbation step-size and perturbation frequency. However, the relation developed is susceptible under severe change in irradiance. The algorithm performance depends on the system parameters which must be carefully modelled and designed. Moreover, the algorithm is sensitive to noise. In [13], the authors used an iterative algorithm that calculates the scaling parameter by using the first and second-order derivatives of the P-V curve. Again, to obtain a scaling parameter for a wide range of irradiance is difficult. In [14], the authors used the circular analogy on the P-V characteristics to determine an approximate optimal location close to MPP. However, the algorithm is computationally intensive especially for implementation in low cost processors.

It is well known that conventional and adaptive MPPT algorithms deviate (drift) from the MPP tracking path under fast changes in irradiance which results in power loss. This deviation is because the algorithm cannot determine the cause behind the change in power. As the conventional MPPT algorithms cannot detect a change in irradiance, these algorithms assume that the change in power is due to intentional perturbation and increases the perturbation in the same direction, which results in power loss. This deviation is severe in adaptive algorithms, as the algorithm uses a large step-size corresponding to a large change in irradiance [15], [16].

Many MPPT techniques have been developed that efficiently determine a sudden variation in irradiance [17]–[20]. In [17], the authors developed a voltage-based MPPT technique by charging and discharging the input capacitor of PV inverter. This technique compares the present and past values of the capacitor voltage to detect a change in irradiance. Although, this technique performs well under uniform irradiance but has a low tracking speed compared to other state-of-the-art algorithms under fast variation in irradiance. Moreover the technique results in substantial power oscillations around MPP. In [18], the authors observed the sign of power change for three consecutive iterations. The algorithm uses two threshold values for variation in power to detect the change in irradiance on the assumption that the MPP does not move substantially during irradiance change. In [19], the algorithm checks the sign of power, voltage and current to deduce sudden variation in irradiance. However, the algorithm deviates from the MPP tracking path if there is a concurrent change in irradiance and load resistance, which is further discussed in Section II. In [20], the authors proposed a multisampling based P&O technique which applies increment, decrement and increment in the step-size in the first, second and third sampling periods, respectively. The algorithm is slow during startup as it needs to perform three iterations. Although,

the algorithm tracks in the right direction. However, in few cases under rapidly changing irradiance the same steps are required to be set consecutively to reach the MPP.

Many other sophisticated MPPT techniques based on artificial neural network, fuzzy logic, grey wolf optimization, particle swarm optimization, firefly algorithm, JayaDe have been developed [21]–[25]. These techniques, although accurate, require large memory, extensive computation, and powerful DSP processors for the increased computational burden. Thus, these techniques are generally used for locating global MPP during partial shading conditions.

As previously mentioned, the main challenge in MPPT algorithms is to follow the correct tracking path under sudden changes in irradiance. Although, there are several MPPT algorithms present in the literature that have good tracking capability under sudden variations in irradiance. However, the performance of these drift-free MPPT techniques remains rather unknown when they are subjected to simultaneous sudden changes in both irradiance and load resistance. In [26], the authors have examined the performance of MPPT algorithm under simultaneous sudden increase in both irradiance and load resistance. But, this case study does not reveal much information as the condition of simultaneous sudden increase in both irradiance and load resistance is similar to the case when there is a sudden change in irradiance with constant load resistance. This is because in both cases the point of operation of next perturbation is on the right side of MPP. In both these cases, the drift-free MPPT algorithms continues to track in the right direction as these algorithms can detect a change in irradiance. However, drift-free MPPT algorithms can lose their tracking capability if there is a simultaneous sudden increase in irradiance and decrease in load resistance, as the operating of the next perturbation will now be on the left side of MPP.

Evidently, in MPPT a change in load resistance has no effect on the performance of the algorithm. But, this is only true when the load resistance is changing under a constant irradiance condition. On the other hand, under simultaneous large variations in irradiance and load resistance, both adaptive and drift-free MPPT algorithms can lose their tracking capability. To date the MPPT algorithms have not been tested for the cases in which a simultaneous sudden change in irradiance and load resistance can result in deviations from their MPP tracking path. Hence, there exists a research gap on the development of a sophisticated MPPT algorithm which performs well regardless of independent or contemporaneous sudden changes in both irradiance and load resistance.

The key novelty features of the proposed algorithm are:

- i) The use of dual perturbation parameters (current and voltage) to increase the speed of tracking by only reducing the current or voltage references from their perturbation step-size.
- ii) The development of perturbation step-size reduction algorithm which iteratively reduces the step-size to limit the steady-state power oscillations. The perturbation step-size reduction algorithm is terminated when the minimum allowable per unit change in voltage or current is reached to prevent false reading in the processor.

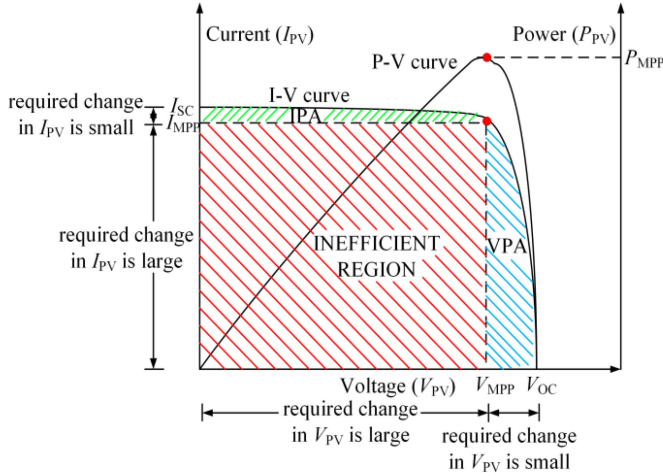


Fig. 1. Operating region of IPA and VPA.

- iii) The use of a deviation avoidance loop which accurately detects independent or concurrent sudden changes in irradiance and load resistance.

As already discussed, an MPPT technique should: have high tracking speed, maintain low power losses during steady-state and should follow the correct tracking path regardless of independent or contemporaneous sudden variations in irradiance and load resistance. To achieve this the proposed algorithm is mainly divided into three parts.

## II. PROPOSED MPPT ALGORITHM

### A. Voltage/Current Perturbation Algorithm (VPA/IPA)

The duty-based or voltage reference or current reference control based P&O algorithm requires several iterations to reach MPP as the point of operation travels through the inefficient region (red region), which slows down the speed of tracking as shown in Fig. 1. The proposed algorithm uses both voltage and current perturbations to ensure that the algorithm never travels through this inefficient region. The use of VPA is similar to voltage reference control based P&O algorithm, i.e., the MPP is tracked using voltage as a control variable, except it is only triggered if the point of operation lies on the right-hand side (RHS) of P-V curve (blue region). The point of operation is in the constant voltage region when  $dP_{PV}/dV_{PV} < 0$ , as shown in Fig. 1. Similarly, IPA is similar to the current reference control based P&O algorithm, except it is triggered if the point of operation lies on the left-hand side (LHS) of the P-V curve (green region). The point of operation is in the constant current region when  $dP_{PV}/dV_{PV} > 0$  as depicted by the I-V curve of Fig. 1, where  $dP_{PV}$  is the change in power and  $dV_{PV}$  the change voltage between two iterations. It is interesting to note that in both VPA and IPA, the perturbation step-sizes are only decremented to reach the MPP.

Therefore, the reference values of VPA or IPA for the next iteration are generated by decrementing the voltage or current perturbation step-size from the previous iteration value of voltage or current, respectively, as in (1) and (2).

$$V_{\text{ref}}(k) = V_{PV}(k-1) - (\Delta V \times V_{PV}(k-1)) \quad (1)$$

$$I_{\text{ref}}(k) = I_{PV}(k-1) - (\Delta I \times I_{PV}(k-1)) \quad (2)$$

where,  $V_{\text{ref}}(k)/I_{\text{ref}}(k)$  is the reference value of voltage/current at  $k^{\text{th}}$  iteration,  $V_{PV}(k-1)/I_{PV}(k-1)$  is the voltage/current of PV at  $(k-1)^{\text{th}}$  iteration and  $\Delta V/\Delta I$  is perturbation step-size of VPA/IPA, respectively.

The operating range of VPA and IPA is in (3) and (4), respectively.

$$V_{\text{MPP}} \leq V_{PV}(k) < V_{\text{OC}} \quad (3)$$

$$I_{\text{MPP}} \leq I_{PV}(k) < I_{\text{SC}} \quad (4)$$

where,  $V_{\text{MPP}}$ ,  $V_{PV}(k)$  and  $V_{\text{OC}}$  is the voltage at: MPP,  $k^{\text{th}}$  iteration and open-circuit, respectively.  $I_{\text{MPP}}$ ,  $I_{PV}(k)$  and  $I_{\text{SC}}$  is the current at MPP,  $k^{\text{th}}$  iteration and short-circuit, respectively.

As depicted in Fig. 1, one can reach MPP with a fewer number of iterations by VPA/IPA if the point operation lies in the blue/green region. Hence, high speed of tracking can be achieved by using both voltage and current reference-based control as they do not operate in the inefficient region of the I-V characteristic, as shown in Fig. 1.

By extensive probing, one can determine the optimum perturbation step-size of VPA and IPA that gives a satisfactory tracking speed while also maintaining the power oscillations to an acceptable level. However, to ensure the generality of the proposed algorithm for different PV arrays and to further reduce the power oscillations under steady-state, the authors used a perturbation step-size reduction algorithm.

### B. Perturbation Step-Size Reduction Algorithm

Initially, the proposed algorithm uses the maximum perturbation step for both voltage and current reference-based algorithms. The maximum starting step-sizes of  $\Delta I = 10\%$  and  $\Delta V = 20\%$  of the instantaneous values of current and voltage, respectively, are chosen by keeping in mind the relations as in (5) and (6), respectively. These relations, although not very accurate, give a good estimate to determine the starting step-size of the proposed algorithm.

$$I_{\text{MPP}} = I_{\text{SC}} \times 0.9 \quad (5)$$

$$V_{\text{MPP}} = V_{\text{OC}} \times 0.8 \quad (6)$$

The difference in step-sizes of IPA and VPA is also because a small reduction in the instantaneous values of current is necessary for IPA to reach MPP. In contrast, a relatively large decrement is required in the instantaneous values of voltage for VPA to reach MPP. The area of constant voltage region (blue region) is comparatively large as compared to the area of the constant current region (green region) as shown in Fig. 1. These step-sizes hold for a single PV module. The generalized equations of maximum perturbation step-sizes for IPA and VPA under start-up for a PV array are given in (7) and (8), respectively.

$$\Delta I_{\text{MAX}} = \frac{\Delta I}{N_P} \quad (7)$$

$$\Delta V_{\text{MAX}} = \frac{\Delta V}{N_S} \quad (8)$$

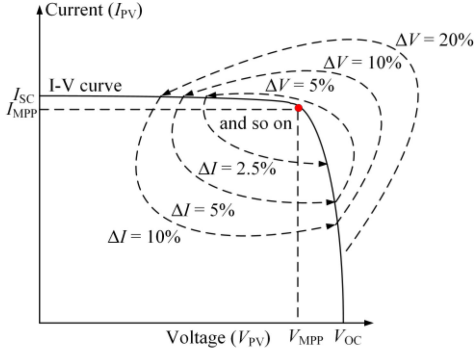


Fig. 2. Iterative reduction of perturbation step-size.

where,  $\Delta I = 10$ ,  $\Delta V = 20$ ,  $N_P$  = number of PV strings in parallel and  $N_S$  = number of PV modules in series.

During start-up, the proposed algorithm uses the maximum step-sizes, which ensures the algorithm to converge towards MPP quickly. However, due to these large starting step-sizes, the algorithm suffers from large oscillations. In the proposed perturbation step-size reduction algorithm, the voltage or current perturbation step-size of the present iteration ( $k^{\text{th}}$ ) is reduced to half of the perturbation step-size of the previous iteration ( $(k-1)^{\text{th}}$ ) after each run of VPA or IPA. Hence, the step-sizes in VPA are iteratively reduced from 20% to 10% to 5% and so on. In IPA, the step-sizes are reduced from 10% to 5% to 2.5% and so on for a single PV module, as depicted in Fig. 2. By decreasing the perturbation step, power oscillations around MPP are drastically reduced. After each operation of VPA/IPA, the voltage/current perturbation step-size is reduced until the desired minimum step-size is obtained. The minimum perturbation step-size ( $\Delta I$  or  $\Delta V$ ) is achieved when the variation in voltage ( $dV_{PV}$ ) and current ( $dI_{PV}$ ) due to perturbation is less than or equal to 1% of the previous iteration value of voltage ( $V_{PV}(k-1)$ ) and current ( $I_{PV}(k-1)$ ), respectively, as in (9) and (10), respectively. This condition is to ensure that the minimum resolution of the analog to digital converter (ADC) of the controller does not come in question, and the controller can easily read the variation in voltage and current due to perturbation.

It is important to mention here that the perturbation step-sizes are reset to their initial values when the algorithm detects a sudden change in irradiance.

$$\left| \frac{dI_{PV}}{I_{PV}(k-1)} \times 100 \right| \leq 1 \quad (9)$$

$$\left| \frac{dV_{PV}}{V_{PV}(k-1)} \times 100 \right| \leq 1 \quad (10)$$

The use of IPA/VPA and PSSRA can help the proposed algorithm to quickly reach MPP with reduced oscillations. However, the algorithm can deviate under simultaneous change in irradiance and load resistance. Hence, a deviation avoidance loop is developed. In the subsequent section, the deviation avoidance loop which detects simultaneous or independent sudden changes in irradiance and load resistance, is discussed.

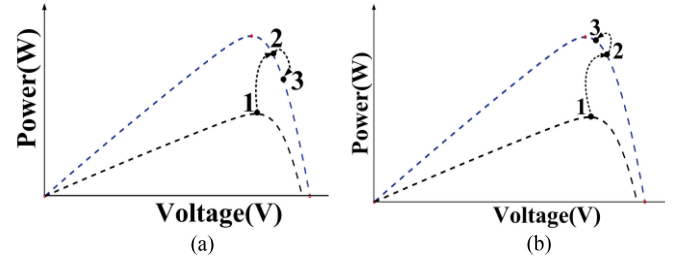


Fig. 3. Point of operation under sudden increase in irradiance (a) moving away from MPP (b) moving towards MPP.

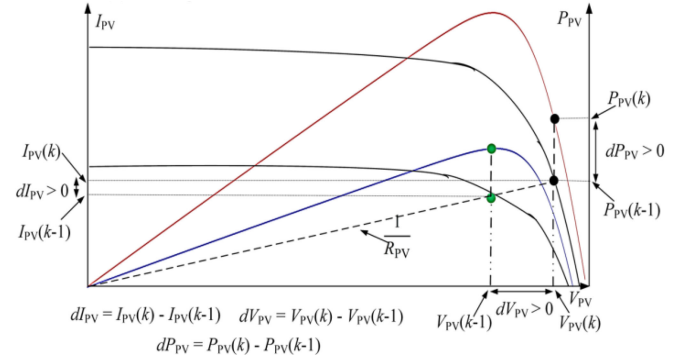


Fig. 4. Slope of power curves P-V and P-I under sudden increase in irradiance.

### C. Deviation Avoidance Loop

It is well known, under rapidly changing irradiance, the P&O algorithm deviates from the ideal tracking path resulting in substantial power loss, as shown in Fig. 3(a). In [8], [19] the algorithms detect a change in irradiance by comparing the sign of change in current and voltage.

1) *Variation in Irradiance*: In deviation avoidance loop, the proposed algorithm detects a change in irradiance by comparing the sign of the gradient of the P-V and P-I power curves. This is because the proposed algorithm uses IPA/VPA and the gradient of power curve can be used to determine the location of the operating point, i.e., left or right of MPP.

During normal operating conditions, the gradient of the power curves, P-V and P-I are of opposite sign. However, under a sudden increase or decrease in irradiance, the sign of the slope of both power curves will be positive or negative. This can be proved by carefully analyzing Fig. 4.

Consider that the MPPT algorithm is currently operating close to the MPP of the low irradiance curve at  $(k-1)^{\text{th}}$  iteration at voltage  $V_{PV}(k-1)$ , current  $I_{PV}(k-1)$  and power  $P_{PV}(k-1)$  as shown in Fig. 4. Assume at this instant there is an increase in irradiance, hence, at  $k^{\text{th}}$  iteration the point of operation will be on the higher irradiance curve at voltage  $V_{PV}(k)$ , current  $I_{PV}(k)$  and power  $P_{PV}(k)$ . This is only true if the load resistance does not change. It is clear from Fig. 4, that change in voltage ( $dV_{PV}$ ), current ( $dI_{PV}$ ) and power ( $dP_{PV}$ ) are positive for an increase in irradiance.

Hence, we can say that sign of  $dP_{PV}/dV_{PV}$  and  $dP_{PV}/dI_{PV}$  is positive only for an increase in irradiance. By checking the

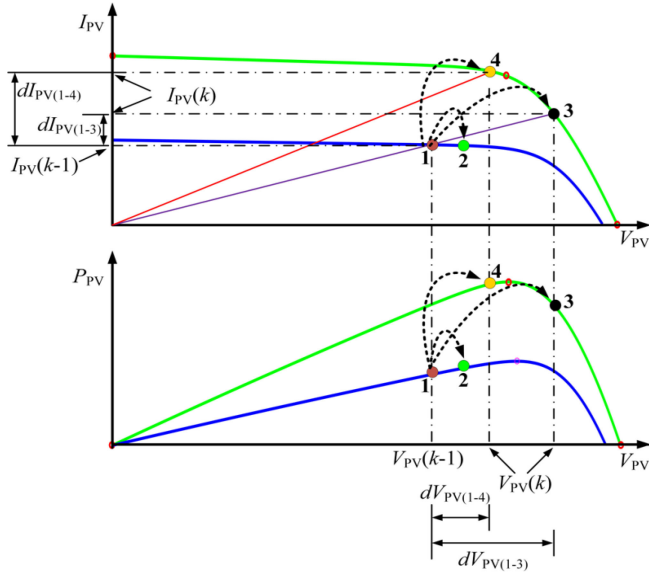


Fig. 5. Shifting of point of operation under a sudden increase in irradiance and load resistance.

sign of the slope of these power curves, the proposed algorithm can detect variation in irradiance. If a sudden rise in irradiance is detected, the operating point of the next iteration will always be on the right-side of MPP of the high irradiance curve, provided the load resistance has increased or remains the same. Hence, the proposed algorithm follows the correct tracking path towards MPP (1→2→3) by applying the voltage perturbation algorithm (VPA), as shown in Fig. 3(b).

It is fascinating to note that even though the algorithm is able to detect a change in irradiance, it may still deviate from the correct MPP tracking path. This condition can occur if there is a sudden increase in both irradiance and decrease in load resistance at the same time.

## 2) Simultaneous Change in Irradiance and Load Resistance:

Let us assume that there is a sudden change in irradiance at  $(k-1)^{\text{th}}$  iteration while going from point 1 to point 2, as shown in Fig. 5.

As explained earlier, if there is a sudden change in irradiance and load resistance increases or remains the same, point of operation at  $k^{\text{th}}$  iteration will be 3. Hence, the point of operation will always be on the right-side of MPP of the higher irradiance curve. Therefore, VPA is triggered, which reduces the voltage and follows the correct MPP tracking path. On the contrary, when there is a simultaneous sudden increase and decrease in irradiance and load resistance, respectively, the point of operation can shift from 1 to 4, if there is a large decrement in the load resistance. In this case, the use of VPA will result in power loss as it decreases the voltage and deviates from the correct MPP path.

To summarize, under a sudden increase in irradiance and a constant load resistance, the operating point will be on right-side of MPP of the higher irradiance curve. On the other hand, there is a good chance that the operating point can shift on the left-side of MPP of the higher irradiance curve if there is a sudden increase

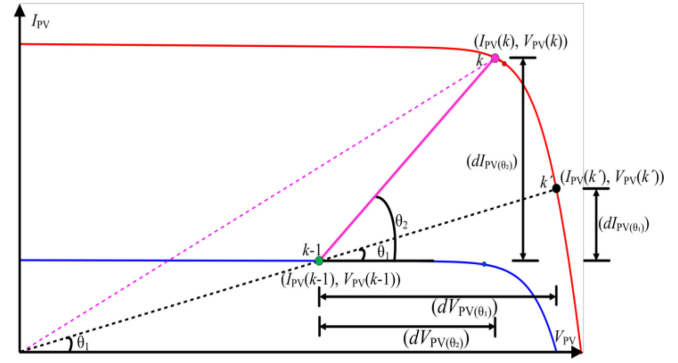


Fig. 6. Comparing gradient to determine a simultaneous change in both irradiance and load resistance.

in irradiance and the load resistance has decreased at the same time.

To determine the location of the operating point of the next iteration, during simultaneous changes in load resistance and irradiance, the proposed algorithm compares the absolute value of the per unit (p.u.) change in current and voltage, as in (11).

$$\left| \frac{dI_{PV}}{I_{PV}(k-1)} \right| \geq \left| \frac{dV_{PV}}{V_{PV}(k-1)} \right| \quad (11)$$

Consider Fig. 5, if the operating point has shifted from 1 to 4, it indicates a simultaneous sudden increase in irradiance and a decrease in load resistance and the point of operation is now on the left-side of MPP of the higher irradiance curve. Here, the p.u. increment in current  $(dI_{PV(1-4)})/I_{PV}(k-1)$  is greater than the p.u. increment in voltage  $(dV_{PV(1-4)})/V_{PV}(k-1)$  as evident from Fig. 5. Hence, IPA is selected to track the MPP.

On the contrary, if the operating point has shifted from 1 to 3, the p.u. increment in voltage  $(dV_{PV(1-3)})/V_{PV}(k-1)$  is greater than the p.u. change in current  $(dI_{PV(1-3)})/I_{PV}(k-1)$ . This shift in the operating point from the left side of MPP of the low irradiance curve to the right-side of MPP of the higher irradiance curve delineates only a change in irradiance while the load resistance remains unchanged. In this case, the MPP is tracked using VPA.

To elaborate this concept, two different scenarios are examined: (i) when there is a sudden increase in irradiance while the load resistance remains unchanged and (ii) when there is a simultaneous sudden increase in irradiance and decrease in load resistance, as shown in Fig. 6.

For the first case, suppose there is only an increase in irradiance while the load resistance remains unchanged. Hence, the operating point will be shifted from green,  $(k-1)^{\text{th}}$  iteration to black,  $(k^{\text{th}})$  iteration. The gradient calculated at both iterations remains the same as the load resistance has not changed as given in (12).

$$\frac{I_{PV}(k-1)}{V_{PV}(k-1)} = \frac{I_{PV}(k') - I_{PV}(k-1)}{V_{PV}(k') - V_{PV}(k-1)} = \frac{dI_{PV(\theta_1)}}{dV_{PV(\theta_1)}} \quad (12)$$

where,  $I_{PV}(k-1)/I_{PV}(k')$  and  $V_{PV}(k-1)/V_{PV}(k')$  is the current and voltage at  $(k-1)^{\text{th}}/(k^{\text{th}})$  iteration, respectively.

TABLE I  
ALGORITHM SELECTION UNDER SUDDEN VARIATIONS IN IRRADIANCE AND  
LOAD RESISTANCE

Variation in Irradiance	Variation in Load Resistance	Algorithm
Increase	Decrease	IPA
Increase	Increase/No change	VPA
Decrease	Decrease/No change	IPA
Decrease	Increase	VPA

$dI_{PV(\theta_1)}$  and  $dV_{PV(\theta_1)}$  is the change in current and voltage observed from  $(k-1)^{\text{th}}$  to  $(k^{\text{th}})$ .

In the second case, there is a simultaneous increase and decrease in irradiance and load resistance, respectively. Hence, the operating point will be shifted from green,  $(k-1)^{\text{th}}$  iteration to pink,  $(k^{\text{th}})$  iteration and the gradient at  $(k^{\text{th}})$  iteration will always be higher compared to the gradient at  $(k-1)^{\text{th}}$  iteration. This increase in gradient indicates that the load resistance has changed as in (13).

$$\frac{I_{PV}(k-1)}{V_{PV}(k-1)} < \frac{I_{PV}(k) - I_{PV}(k-1)}{V_{PV}(k) - V_{PV}(k-1)} = \frac{dI_{PV}(\theta_2)}{dV_{PV}(\theta_2)} \quad (13)$$

Since, both irradiance and load resistance can both increase or decrease the authors have taken the absolute value of (13) to take into account the sign of  $dI_{PV}$  and  $dV_{PV}$ , as the main objective is to determine the per unit change in current and voltage to determine the location of the operating point.

Hence, the comparison between the values of the p.u. change in current and voltage can locate the region of the operating point of the next iteration. It is essential to point out that only a large variation in load resistance is considered for the case studies.

As both irradiance and load resistance may vary, four combinations are possible, which are given in Table I. By including these cases, the proposed algorithm selects VPA or IPA depending upon the region of operating point and tracks in the right direction regardless of concurrent or independent variations in irradiance and load resistance. The flowchart of the proposed algorithm is shown in Fig. 7.

Since direct decrement in voltage and current cannot be attained as the control parameter used is duty [15]. Hence, two independent proportional-integral (PI) controllers are tuned to implement VPA and IPA.

### III. DESIGN OF VOLTAGE AND CURRENT CONTROL LOOP

The measured values of voltage and current are perturbed around their operating point to deduce the small-signal expressions, as discussed in this section.

The MPPT controller determines the voltage or current reference by executing VPA or IPA depending upon the region of operating point right-side or left-side of MPP, respectively, as shown in Fig. 8. Thereby the PWM generator produces a duty cycle corresponding to this reference. The switching device of the DC-DC boost converter is operated at a high switching frequency of 16 kHz. The meticulous design of current and voltage control loop ensures the robustness and stability of the system. The parameters of the boost converter chosen for the investigation are given in Table II.

TABLE II  
PARAMETERS OF BOOST CONVERTER

$V_{PV}$	$I_{PV}$	$V_o$	$d$	$R$	$L$	$C$
17.84 V	4.5 A	40 V	0.554	20 $\Omega$	6 mH	47 $\mu$ F

#### A. Steady State Stability of the Controller

The state equations of the boost converter over a switching cycle are given below in (14) and (15)

$$L \frac{dI_{PV}}{dt} = V_{PV} - (1-d)V_o \quad (14)$$

$$C \frac{dV_o}{dt} = (1-d)I_{PV} - \frac{V_o}{R} \quad (15)$$

where,  $I_{PV}$ ,  $V_{PV}$  and  $V_o$  are input current, input voltage and output voltage of the converter, respectively and  $R$ ,  $L$ ,  $C$  and  $d$  represent the output resistance, inductor, capacitor and duty ratio. By introducing perturbation in input voltage, input current and duty, the transfer functions of control to voltage and control to current are obtained as given in (16) and (17), respectively.

$$G_{vd}(s) = \frac{\tilde{v}_{PV}}{\tilde{d}} = \frac{Cs + \frac{1}{R} - (1-d_0)I_{PV_0}}{LCs^2 + \frac{L}{R}s + (1-d_0)^2} \quad (16)$$

$$G_{id}(s) = \frac{\tilde{i}_{PV}}{\tilde{d}} = \frac{V_{o_0}Cs + \frac{V_{o_0}}{R} + (1-d_0)I_{PV_0}}{LCs^2 + \frac{L}{R}s + (1-d_0)^2} \quad (17)$$

where,  $\tilde{v}_{PV}$ ,  $\tilde{i}_{PV}$  and  $\tilde{d}$  are small perturbations in  $V_{PV}$ ,  $I_{PV}$  and  $d$ , respectively.

The transfer function of the PI controller for voltage and current control loop is given in (18) and (19), respectively.

$$G_v(s) = K_{pv} + \frac{K_{iv}}{s} \quad (18)$$

$$G_c(s) = K_{pc} + \frac{K_{ic}}{s} \quad (19)$$

The open-loop transfer function of voltage and current control loop is given in (20) and (21), respectively.

$$G_{olv}(s) = G_{vd}(s)G_v(s) \quad (20)$$

$$G_{olc}(s) = G_{id}(s)G_c(s) \quad (21)$$

The bode plot and root locus of the voltage and current control loop without and with compensation are shown in Fig. 9(a)–(b), respectively. Fig. 9(a) shows that the open-loop transfer function has a phase margin of  $-91.4^\circ$  at 16.6 rad/s for voltage control loop and a phase margin of  $81.8^\circ$  at 6.99 krad/s for the current control loop.

Therefore, the voltage PI controller of the closed-loop system is designed to achieve a phase margin of  $60^\circ$  at 7.8 krad/s [27]. The parameters calculated are  $K_{pv} = 0.144$ ,  $K_{iv} = 874.6$ .

The current PI controller of the closed-loop system is designed to achieve a maximum overshoot of 5.86% and to achieve a phase margin of  $60^\circ$  at 1.31 krad/s. The parameters calculated are  $K_{pc} = 0.093$  and  $K_{ic} = 58.69$ . Fig. 9(b) shows that the closed-loop poles of the compensated voltage control loop for the designed phase margin occur at  $p_{1,2} = -532 \pm j650$  ( $\zeta = 0.633$ ,  $\omega_n =$

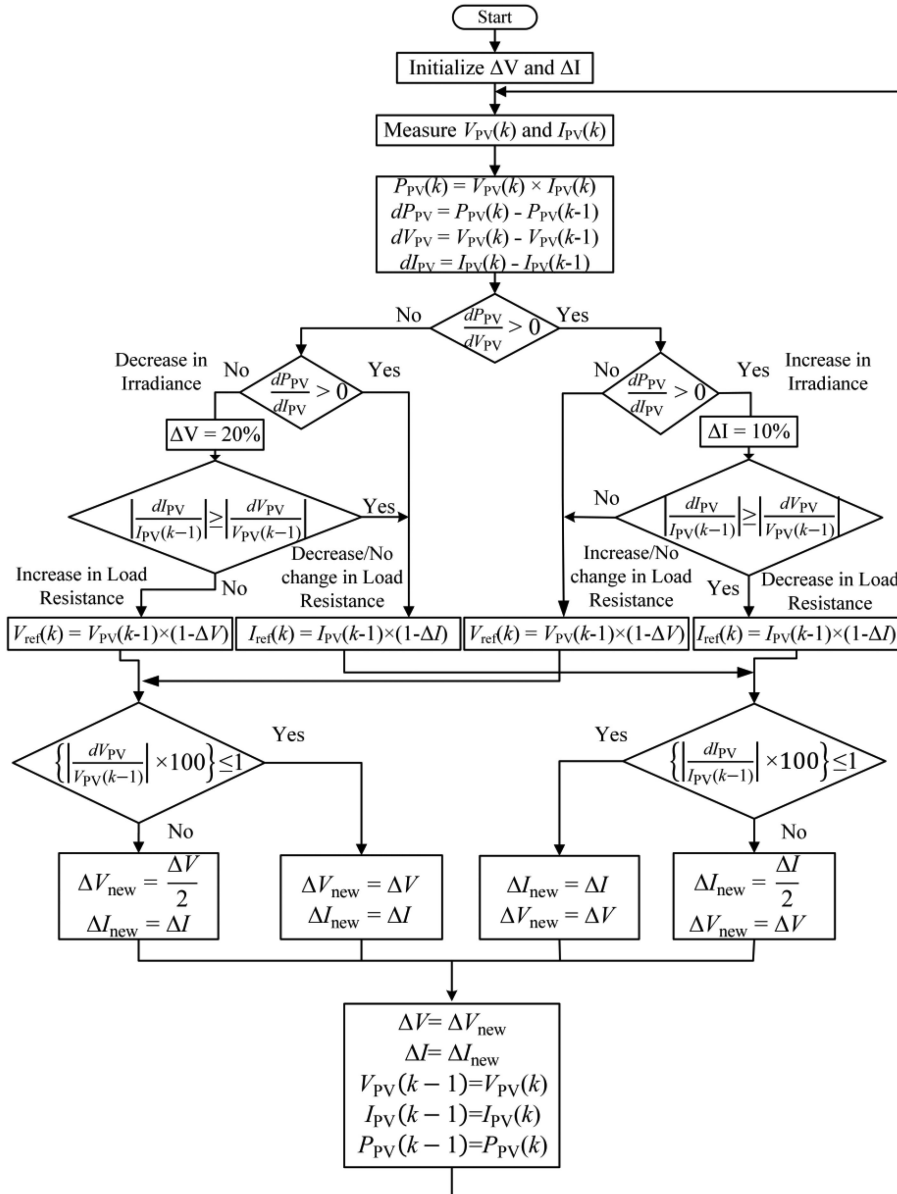


Fig. 7. Flowchart of the proposed algorithm.

840 rad/s). The closed loop-poles of the compensated current control loop for the desired phase margin occur at  $p_1 = 0$  and  $p_{2,3} = -532 \pm j650$  ( $\zeta = 0.633$ ,  $\omega_n = 840$  rad/s), which ensures the stability of the system.

### B. Controller Stability During Transition

When the controller is continuously switching between the VPA and IPA modes, the equivalent transfer function of the boost converter with the associated current and voltage PI controllers are also dynamically changing. To simulate the transition of the controllers in the small-signal domain, the transfer functions which are obtained by state space averaging are linearized around the operating points  $V_o$ ,  $I_{PV_0}$ ,  $V_{PV_0}$  and  $d_0$ . The linearized equations can be seen as

$$\frac{d\tilde{i}_{PV}}{dt} = -\frac{(1-d_0)\tilde{v}_o}{L} + \frac{V_o\tilde{d}}{L} + \frac{\tilde{v}_{PV}}{L} \quad (22)$$

$$\frac{d\tilde{v}_o}{dt} = \frac{(1-d_0)\tilde{i}_{PV}}{C} - \frac{I_{PV_0}\tilde{d}}{C} - \frac{\tilde{v}_o}{RC} \quad (23)$$

The perturbation around the steady-state value in the state variables are given below:

$$V_o = V_{o_0} + \tilde{v}_o \quad (24)$$

$$I_{PV} = I_{PV_0} + \tilde{i}_{PV} \quad (25)$$

$$V_{PV} = V_{PV_0} + \tilde{v}_{PV} \quad (26)$$

$$d = d_0 + \tilde{d} \quad (27)$$

where,  $\tilde{v}_o$ ,  $\tilde{i}_{PV}$ ,  $\tilde{v}_{PV}$  and  $\tilde{d}$  are perturbations in the output voltage, input current, input voltage and duty ratio, respectively. The block diagram obtained from (22) and (23) along with the voltage and current PI controllers is shown in Fig. 10.

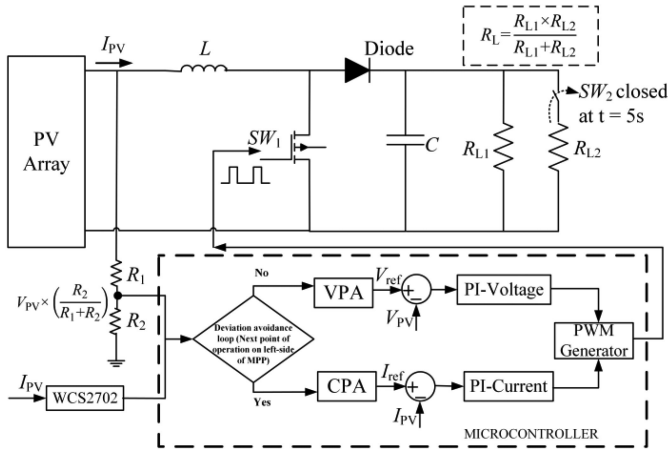


Fig. 8. Circuit diagram of the proposed MPPT controller.

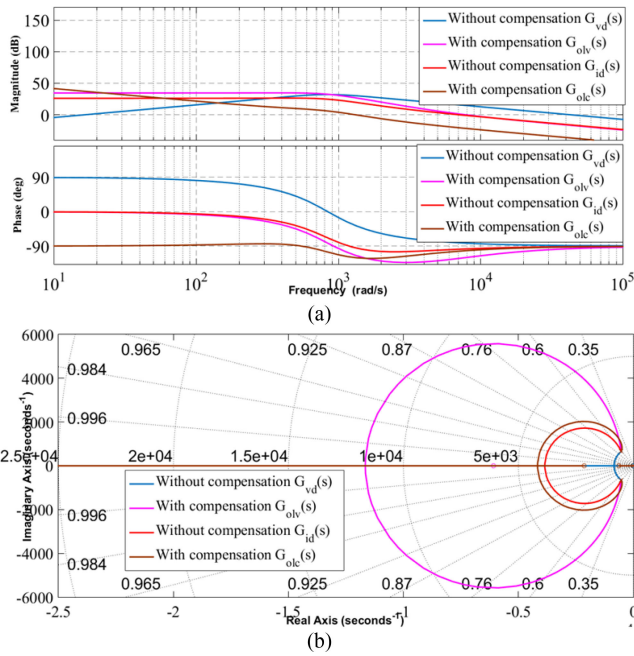


Fig. 9. Voltage and current control loop with and without compensation (a) Bode plot and (b) Root locus.

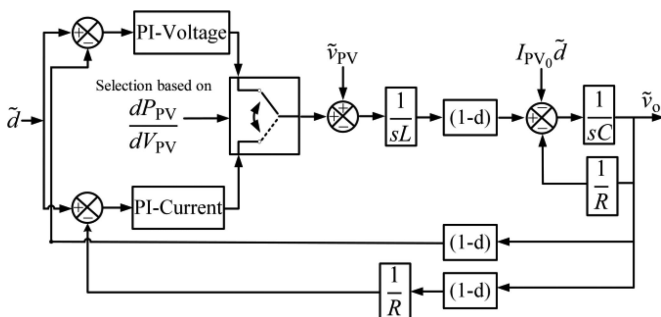


Fig. 10. Block diagram of the linearized small-signal model.

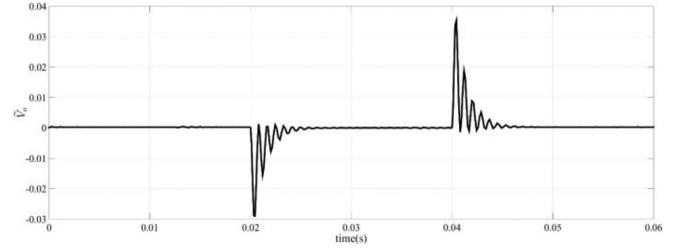


Fig. 11. Response during transition between the voltage and current operating mode.

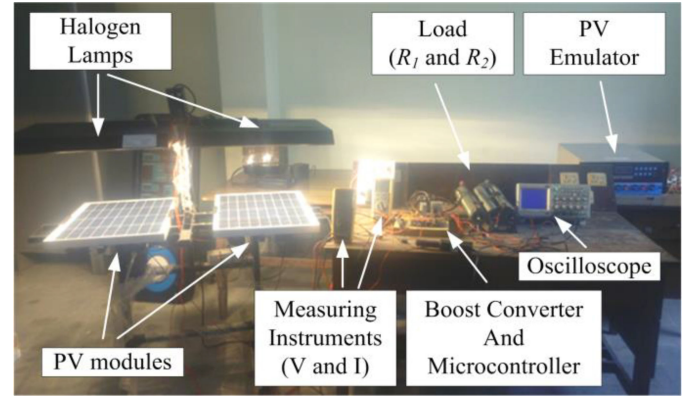


Fig. 12. Small scale prototype of MPPT controller.

It can be observed that when the controller is switching between the two algorithms, the transfer function is altered, and the small signal response is generated by providing an exogenous disturbance in  $I_{PV}$ ,  $V_{PV}$  and  $d$ . As we are looking at small signal disturbance, a '0' input is provided to the controller, and the controller is switched on the basis of the current and the voltage perturbations which are applied in the actual MPPT model, while transitioning between IPA and VPA.

To determine the stability during dynamic transition between voltage and current controllers, the authors have taken two cases, i.e., while going from IPA to VPA and vice versa.

- Initially at  $t = 0$  s, IPA is operational. Then at  $t_1 = 0.02$  s, a  $\frac{dP_{PV}}{dV_{PV}} < 0$  condition is emulated to initiate a transition to VPA, as shown in Fig. 10.
- After some time at  $t_2 = 0.04$ s, transition from VPA to IPA occurs when  $\frac{dP_{PV}}{dV_{PV}} > 0$ .

As shown in Fig. 11, the transitions from IPA to VPA and vice versa are stable due to the tuned values of the controllers mentioned in the previous sub-section. An undershoot peak of 0.029 V is observed in the response of  $\tilde{v}_o$  at 0.02 s. On the other hand, an overshoot peak of 0.035 V is recorded for the same signal at 0.04 s. In both the cases, the response time to reach steady-state was around 5 ms.

#### IV. EXPERIMENTAL RESULTS

A small-scale experimental prototype shown in Fig. 12 is used to implement the proposed algorithm. The proposed algorithm is tested on a programmable Ecosense PV emulator



TABLE III  
SPECIFICATIONS OF ELDORA40P PV MODULE AT STC

$V_{OC}$	$I_{SC}$	$V_{MPP}$	$I_{MPP}$	$\beta_{OC}$	$\alpha_{SC}$
21.95V	2.44A	17.84V	2.25A	-0.31V/°C	0.058A/°C

(IGE-PV4C400-001) as well as on a Vikram Solar 40W polycrystalline PV module (ELDORA 40P). The specification of the PV module is in Table III. The current sensor (WCS2702) is used to measure module current, while voltage is sensed of a potential divider. The MPPT algorithm is programmed in a cost-effective ATMEGA-32 microcontroller of a 10-bit ADC. A DC-DC boost converter is designed to implement the algorithm. Two rheostats having a range of  $300\Omega$  are connected in parallel as a load to investigate the reliability of the proposed algorithm under varying load resistance. Fluke 287 multi-meters and TDS2000C digital storage oscilloscope are used to store the experimental data in .csv format. These .csv data files are then read in MATLAB/Simulink environment. The voltage, current and power response of the tested MPPT algorithms is then traced with their ideal waveforms.

#### A. Selection of State-of-the-Art Algorithms for Comparison

The performance of the proposed algorithm is evaluated using two case studies. In the first case, the efficiency of the tested algorithms is evaluated using a standard EN50530 irradiance profile [28]. In the second case, the performance of the algorithm is determined under simultaneous sudden changes in irradiance and load resistance. The selection of state-of-the-art algorithms for comparison with the proposed algorithm in the two case studies are given next.

1) *State-of-the-Art Algorithms Under EN50530 Test:* For the first case study, the performance of the proposed algorithm is determined under EN50530 irradiance profile and a constant load resistance. For comparison, the authors selected two state-of-the-art algorithms: low-cost incremental conductance (LCInC) of [10] and an adaptive step-size (ASS) algorithm of [13] which have been compared with the conventional P&O algorithm.

where,  $V_{OC}$ ,  $I_{SC}$ ,  $V_{MPP}/I_{MPP}$ ,  $\beta_{OC}/\alpha_{SC}$  is the open-circuit voltage, short-circuit current, maximum power point voltage/current and temperature coefficient of voltage/current of the PV module, respectively.

The LCInC algorithm of [10] showed superior performance than the conventional P&O algorithm under a step change in irradiance. On the other hand, the adaptive step-size algorithm of [13] had an excellent dynamic response and uses an adaptive step-size to converge towards MPP within a small number of iterations. Since these algorithms have already proven their efficacy over the conventional P&O algorithm, the comparison with the conventional P&O algorithm is not conducted

2) *State-of-the-Art Algorithm Under Simultaneous Sudden Change in Irradiance and Load Resistance:* As previously mentioned, several widely popular drift-free MPPT algorithms can be found in the literature that works well under sudden variations in irradiance levels. But, very few researchers have investigated

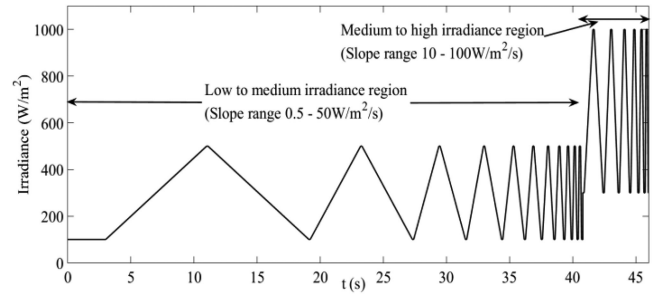


Fig. 13. EN50530 Irradiance profile for the experimental study.

the performance of these drift-free MPPT algorithms when they are subjected to sudden variations in both irradiance and load resistance at the same time [26]. However, the authors in [26] have not investigated the explicit case scenarios where the drift-free algorithms can fail if there is a instantaneous sudden change in both irradiance and load resistance.

Therefore, the behavior response of these drift-free MPPT techniques still remain rather unknown when there is a concurrent sudden change in both irradiance and load resistance.

The authors have determined the effectiveness of the proposed algorithm under simultaneous sudden change in irradiance and load resistance by comparing it with a widely popular drift-free MPPT algorithm of [2] to clearly demonstrate the events where these drift-free algorithms can fail. In [2], the authors proposed a voltage-based drift-free MPPT algorithm that follows the correct MPP path due to its ability to accurately detect sudden changes in irradiance. Therefore, the authors have compared the performance of the proposed algorithm with this recently developed drift-free MPPT algorithm of [2] in the second case study.

#### B. Case Study 1: EN50530 Irradiance Profile

The PV emulator is used to generate EN50530 irradiance profile. The PV emulator used has four modes of operation, namely fixed, table, simulator and programming mode. An offline table was developed containing the voltage and current values of the ELDORA40P 40W PV module specifications corresponding to each irradiance and temperature level. This table was then used to construct the EN50530 irradiance test profile which was programmed in the PV emulator.

The response of the proposed algorithm is compared with low-cost incremental conductance (LCInC) [10] and adaptive step-size algorithm (ASS) [13] under EN50530 irradiance profile, shown in Fig. 13. The low to medium irradiance region is between  $100 \text{ W/m}^2$  to  $500 \text{ W/m}^2$  whereas, the medium to high irradiance region ranges from  $300 \text{ W/m}^2$  to  $1000 \text{ W/m}^2$ .

A step-size of  $\Delta D_{LCInC} = 0.5\%$  is selected for LCInC algorithm. This is because the ADC can easily detect the variation in voltage and current due to this step-size. Moreover, voltage variation due to this step-size is much greater than the voltage magnitude of the inherent switching ripple of the converter. An initial operating voltage of  $V_{ini} = 0.95 \times V_{OC}$  is selected for the ASS algorithm. Then this voltage is decremented by taking an initial step-size of  $\Delta V_{ASS} = 0.05 \times V_{OC}$  as suggested in [13].

TABLE IV  
COMPARISON BETWEEN MPPT ALGORITHMS

Algorithm	Efficiency under EN50530 irradiance profile			$t_{ss}$ under simultaneous sudden variations in both irradiance and load resistance			
	Efficiency under 0.5W/m <sup>2</sup> /s	Efficiency under 100W/m <sup>2</sup> /s	Overall efficiency	$t_{ss}$ under start-up	$t_{ss}$ under sudden increase in irradiance and decrease in load resistance	$t_{ss}$ under sudden decrease in irradiance and increase in load resistance	Possibility of deviation from MPP tracking path under simultaneous change in irradiance and load resistance?
LCInC [10]	98.56%	93.35%	97.76%	185 ms	140 ms	135 ms	Low
Adaptive Step-Size [13]	98.67%	92.89%	98.15%	130 ms	115 ms	100 ms	High
Voltage-based Drift-Free [2]	98.70%	95.90%	98.53%	150 ms	280 ms	170 ms	High
Proposed	98.75%	98.89%	98.85%	80 ms	55 ms	80 ms	No

For the proposed algorithm, the maximum starting step-size of  $\Delta I = 5\%$  and  $\Delta V = 20\%$  for IPA and VPA are calculated using (11) and (12), respectively. PSSRA reduces the step-size after each successive iteration.

When the minimum step-size of  $\Delta V_{MIN} = 0.625\%$  for VPA and  $\Delta I_{MIN} = 2.5\%$  for IPA is reached no more reduction in step-size takes place. This is done to ensure that the change in voltage and change in current due to perturbation does not fall below the preset limit of  $dV_{PV} = 0.1V$  and  $dI_{PV} = 0.01A$ , respectively which is higher than the minimum resolution of the analog to digital converter (ADC) of the controller.

### C. Case Study 2: Simultaneous Sudden Change in Irradiance and Load Resistance

The dynamic performance of the proposed algorithm is compared with another recently developed state-of-the-art voltage-based drift-free P&O algorithm of [2] under simultaneous variations in irradiance and load resistance.

Both the algorithms are tested on an 80W PV array formed by connecting two 40 W PV modules in series. In this case, the irradiance is suddenly varied over the PV array (instead of the PV emulator) by using artificial lighting provided by 150 W halogen lamps.

In this test case, the array is operated under relatively steady temperature range by using fans installed at the bottom of the PV modules,  $T = 25^\circ C$  to  $25.5^\circ C$ . At  $t < 0$  s, the PV works in the load following mode, keeping the duty cycle at 0.

At  $t_1 = 0$  s, the  $SW_2$  is turned off and the algorithms are activated in succession with a starting irradiance of  $G = 270$  W/m<sup>2</sup>, with a load resistance,  $R_L = 260 \Omega$ , as shown in Fig. 8. At  $t_2 = 5$  s, the irradiance is instantly increased to 480 W/m<sup>2</sup> and the load resistance decreased to  $R_L = 130 \Omega$  at the same instance by turning  $SW_2$  on. The decrease in resistance from 260  $\Omega$  to 130  $\Omega$  ensures the point of operation shifts from the positive slope of 270 W/m<sup>2</sup> P-V curve to the positive slope of 480W/m<sup>2</sup> P-V curve. After some time at  $t_3 = 10$  s, the irradiance is reduced back to 270W/m<sup>2</sup> and load resistance is increased back to  $R_L = 260\Omega$ . A step-size of  $\Delta V = 0.5V$  is taken for voltage-based drift-free P&O algorithm as suggested in [2], whereas maximum starting step-size of  $\Delta I = 5\%$  and  $\Delta V = 20\%$  for IPA and VPA are selected as done in the first case study.

### D. Comparison Between the Proposed and State-of-the-Art Algorithms

The overall comparison between the tested algorithms is carried out based on the following key performance indices as shown in Table IV.

1) *Efficiency*: The dynamic efficiency under EN50530 irradiance test profile is calculated using (28) as in [20]. The dynamic efficiencies of the tested algorithms are given in Table IV.

$$\% \text{ Dynamic Efficiency} = \frac{\text{power extracted}}{\text{ideal power}} = \frac{\int_0^T V_{PV} \times I_{PV}}{\int_0^T P_{MPP}} \quad (28)$$

where, T is the test period.

The response curves of LCInC [10], ASS [13] and the proposed algorithm operating under EN50530 irradiance profile are shown in Fig. 14(a)–(f), respectively. For a slow change in irradiance (0.5W/m<sup>2</sup>/s) operating in low to medium region, the LCInC [10], adaptive step-size of [13] and the proposed algorithm behave quite similarly to each other, except for minor changes in steady-state power oscillations.

In medium to large irradiance region, under steep slopes of changing irradiance (100W/m<sup>2</sup>/s) the LCInC algorithm [10] quickly decreases its perturbation step-size when it detects a change in irradiance, to avoid transient power loss. However, due to the fast continuous variation in irradiance the LCInC algorithm gets confused and deviates from the tracking path.

Similarly, the ASS algorithm [13] also shows large deviation from the ideal waveform. This is because the ASS algorithm adaptively changes the step-size when it observes a large change in power to increase the convergence speed towards MPP. The zoomed response curves of LCInC and ASS algorithm are shown in Fig. 14(b) and Fig. 14(d), respectively. On the contrary, the proposed algorithm identifies the variation in irradiance by comparing the sign of the slope of P-V and P-I curves and does not deviate from the MPP tracking path and tracks with high efficiency, as shown in Fig. 14(e)–(f). The dynamic efficiency of the algorithms evaluated for gradually and rapidly changing irradiance with a slope of 0.5 W/m<sup>2</sup>/s and 100 W/m<sup>2</sup>/s, respectively is given in Table IV.

2) *Response Time to Reach Steady-State at MPP ( $t_{ss}$ )*: The speed of MPP tracking is determined by the time taken by the algorithm to reach steady-state ( $t_{ss}$ ) when there is a change in the operating condition.

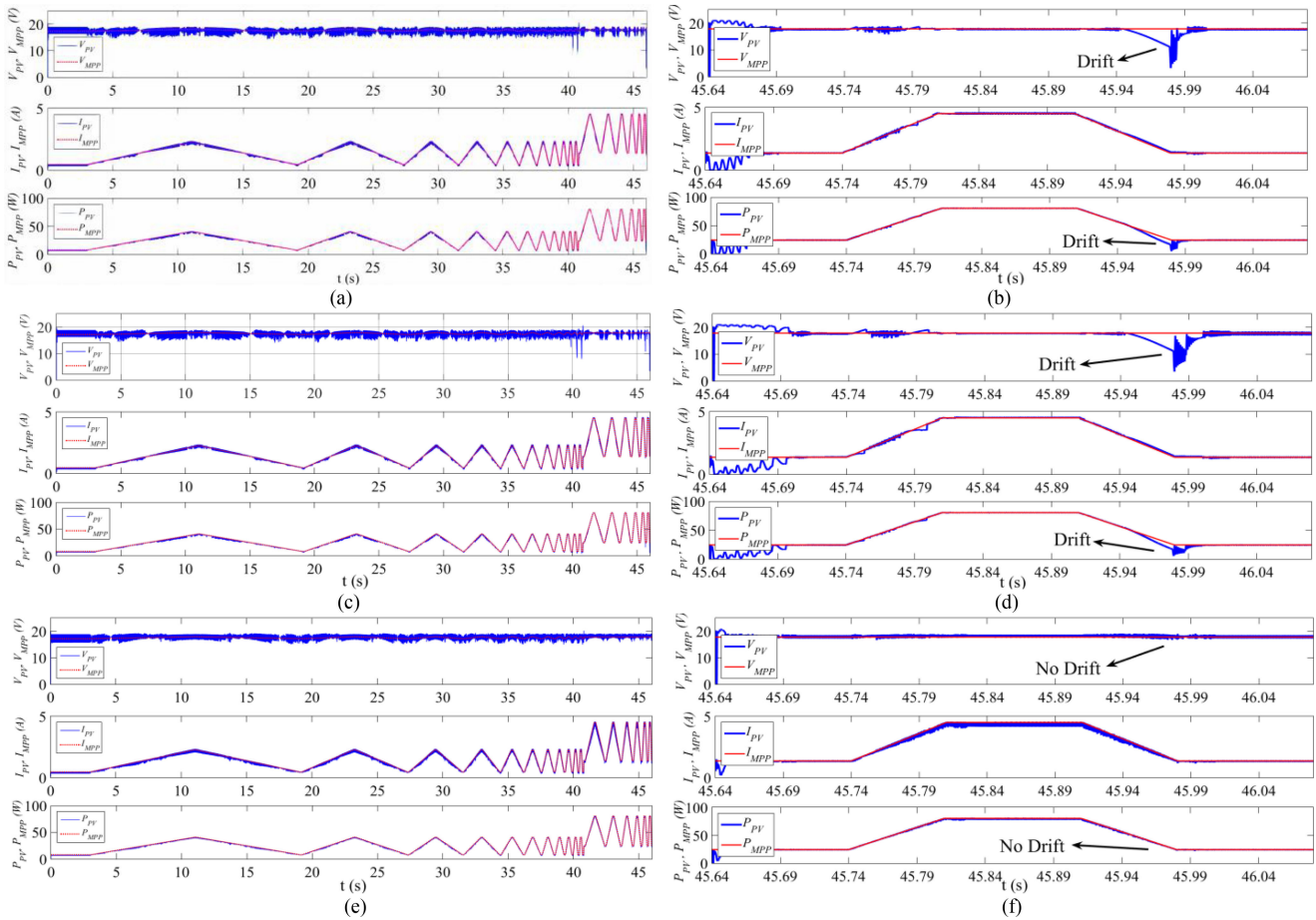


Fig. 14. Response for the complete EN50530 irradiance profile of (a) LCInC [10] (c) ASS [13] and (e) proposed algorithm and zoomed response under rapid change in high values of irradiance with slope of 100W/m<sup>2</sup>/s of (b) LCInC [10], (d) ASS [13] and (f) proposed algorithm.

The voltage-based drift-free of [2] uses an objective function  $Q_1$  to determine an increase or decrease in irradiance level. Once steady state is reached, the sign of  $Q_1$  can accurately detect a change in irradiance. If  $Q_1 > 0$ , the reference voltage is decreased whereas the reference voltage is increased if  $Q_1 < 0$ . The zoomed response curves of the voltage-based drift-free of [2] and proposed algorithm at  $t_2 = 5s$  are shown in Fig. 15(a)–(b), respectively. Since irradiance and load resistance has simultaneously increased and decreased at  $t_2 = 5s$ , the objective function,  $Q_1$  of voltage-based drift-free P&O algorithm is positive, indicating a change in irradiance. Hence, the voltage-based drift-free P&O algorithm of [2] reduces the reference voltage. However, due to the change in load resistance the point of operation is now on the left-side of MPP. Therefore, the voltage-based drift-free P&O algorithm deviates from the MPP tracking path as it tries to decrease the reference voltage, and hence tracks in the wrong direction under a contemporaneous change in irradiance and load resistance as shown in Fig. 15(a). In contrast to this erroneous behavior, the proposed algorithm detects an increase in irradiance by comparing the slope of P-V and P-I curves. Then the proposed algorithm compares the per unit (p.u.) change in current with the p.u. change in voltage to determine the location of the operating point. As the point of operation has shifted from the left-side of low irradiance curve to the left-side of high

irradiance curve, the p.u. change in current is larger than the p.u. change in voltage. Therefore, IPA is triggered and the proposed algorithm follows the correct MPP path. Similarly, at  $t_3 = 10s$ , when the irradiance and load resistance has simultaneously decreased and increased, the point of operation has shifted from the right-side of high irradiance curve to the right-side of low irradiance curve. Here, the p.u. change in voltage is greater than the p.u. change in current. Hence, the proposed algorithm selects VPA and tracks in the right direction. On the contrary, in voltage-based drift-free P&O algorithm,  $Q_1 < 0$ , as there is a decrease in irradiance which results in an increase in the reference voltage and therefore tracks in the wrong direction. The zoomed response curve of voltage-based drift-free P&O and the proposed algorithm at  $t_3 = 10s$  is shown in Fig. 15(c)–(d).

The experimental results show that the proposed algorithm has the highest tracking speed as compared to LCInC [10], ASS [13] and voltage-based drift-free [2]. This is because of the use of both voltage and current control loop having excellent dynamic response as validated from the small-signal stability analysis and tracks the MPP while operating in the efficient region as explained before using Fig. 1. The proposed algorithm compares the slope of P-V and P-I curve to detect a change in irradiance and hence does not deviate from the MPP tracking path under sudden variations in irradiance. The experimental waveforms also verify

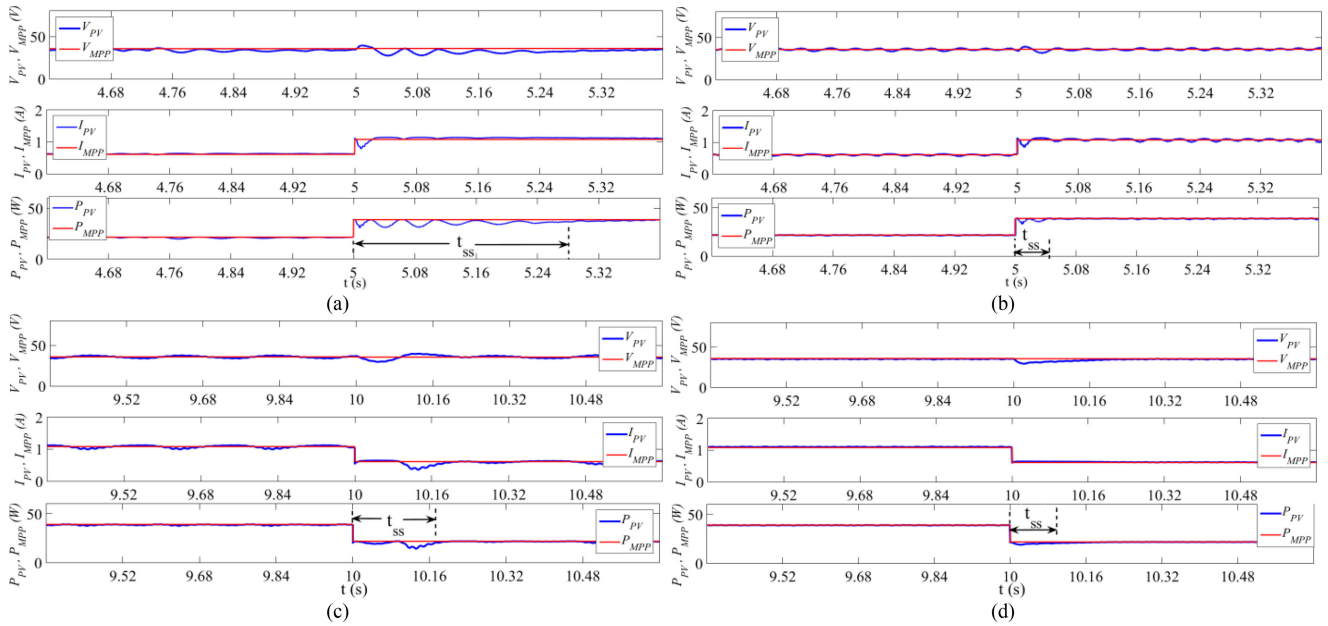


Fig. 15. Zoomed response of (a) Voltage-based Drift-Free P&O [2] and (b) Proposed Algorithm under a simultaneous sudden increase in irradiance and decrease in load resistance; (c) Drift-Free P&O [2] and (d) Proposed Algorithm under simultaneous sudden decrease in irradiance and increase in load resistance.

that the drift-free algorithms deviate from the MPP tracking path when there is a simultaneous sudden increase in irradiance and decrease in load resistance. On the contrary, the proposed algorithm compares the p.u. change in current and voltage using (11) which helps in locating the operating point region of the next iteration. Depending on the region of operation, i.e., right or left side of MPP, the proposed algorithm executes VPA or IPA and can still track in the right direction for all possible conditions of simultaneous sudden variations in irradiance and load resistance.

## V. CONCLUSION

This paper proposes a voltage and current reference-based MPPT technique that works efficiently under varying environmental conditions. The proposed technique uses both current and voltage perturbations to speed up the tracking speed. To minimize steady-state power oscillations, the authors proposed the use of PSSRA, which iteratively reduces the perturbation step-size. The simultaneous variations in both irradiance and load resistance can affect the performance of MPPT algorithms as they can deviate from the tracking path. To overcome this, the proposed algorithm developed a deviation avoidance loop which compares the p.u. change in current and voltage to locate the next point of operation on the P-V curve, under contemporaneous or independent sudden variations in irradiance and load resistance. Once, the location of the operating point is determined, left or right side of MPP, IPA or VPA is selected and follows MPP tracking path without deviation. The proposed technique is implemented using a cost-effective microcontroller and does not require large memory and complex computations.

## REFERENCES

- [1] B. Subudhi and R. Pradhan, "A comparative study on maximum power point tracking techniques for photovoltaic power systems," *IEEE Trans. Sustain. Energy*, vol. 4, no. 1, pp. 89–98, Jan. 2013.
- [2] M. Killi and S. Samanta, "Voltage-sensor-based MPPT for stand-alone PV systems through voltage reference control," *IEEE Trans. Emerg. Sel. Top. Power Electron.*, vol. 7, no. 2, pp. 1399–1407, Aug. 2018.
- [3] A. Pandey, N. Dasgupta, and A. K. Mukerjee, "High-performance algorithms for drift avoidance and fast tracking in solar MPPT system," *IEEE Trans. Energy Convers.*, vol. 23, no. 2, pp. 681–689, Jun. 2008.
- [4] Q. Mei, M. Shan, L. Liu, and J. M. Guerrero, "A novel improved variable step-size incremental-resistance MPPT method for PV systems," *IEEE Trans. Ind. Electron.*, vol. 58, no. 6, pp. 2427–2434, Jun. 2011.
- [5] A. K. Abdelsalam, A. M. Massoud, S. Ahmed, and P. N. Enjeti, "High-Performance adaptive perturb and observe MPPT technique for photovoltaic-based microgrids," *IEEE Trans. Power Electron.*, vol. 26, no. 4, pp. 396–405, Apr. 2011.
- [6] S. K. Kollimalla and M. K. Mishra, "Variable perturbation size adaptive P&O MPPT algorithm for sudden changes in irradiance," *IEEE Trans. Sustain. Energy*, vol. 5, no. 3, pp. 718–728, Jul. 2014.
- [7] R. Gomez-Merchan *et al.*, "Binary search-based flexible power point tracking algorithm for photovoltaic systems," *IEEE Trans. Ind. Electron.*, to be published, doi: [10.1109/TIE.2020.2998743](https://doi.org/10.1109/TIE.2020.2998743).
- [8] T. H. Kwan and X. Wu, "An adaptive scale factor based MPPT algorithm for irradiating solar irradiation levels in outer space," *Acta Astronaut.*, vol. 132, pp. 33–42, Mar. 2017.
- [9] Y. H. Liu, J. Chen, and J. Huang, "Global maximum power point tracking algorithm for PV systems operating under partially shaded conditions using the segmentation search method," *Sol. Energy*, vol. 103, pp. 350–363, May 2014.
- [10] N. E. Zakzouk, M. A. Elsharty, A. K. Abdelsalam, A. A. Helal, and B. W. Williams, "Improved performance low-cost incremental conductance PV MPPT technique," *IET Renewable Power Gener.*, vol. 10, no. 4, pp. 561–574, Apr. 2016.
- [11] H. A. Sher, A. F. Murtaza, A. Noman, K. E. Addoweesh, and K. Al-Haddad, "A new sensorless hybrid MPPT algorithm based on Fractional short-circuit current measurement and P&O MPPT," *IEEE Trans. Sustain. Energy*, vol. 6, no. 4, pp. 1426–1434, Oct. 2015.
- [12] Y. Jiang, J. A. A. Qahouq, and T. A. Haskew, "Adaptive step size with adaptive-perturbation-frequency digital MPPT controller for a single-sensor photovoltaic solar system," *IEEE Trans. Power Electron.*, vol. 28, no. 7, pp. 3195–3205, Jul. 2013.
- [13] L. Tang, W. Xu, and C. Mu, "Analysis for step-size optimisation on MPPT algorithm for photovoltaic systems," *IET Power Electron.*, vol. 10, no. 13, pp. 1647–1654, Nov. 2017.
- [14] N. Kumar, I. Hussain, B. Singh, and B. K. Panigrahi, "Framework of maximum power extraction from solar PV panel using self predictive perturb and observe algorithm," *IEEE Trans. Sustain. Energy*, vol. 9, no. 2, pp. 895–903, Apr. 2018.

- [15] M. A. Elgendy, B. Zahawi, and D. J. Atkinson, "Assessment of perturb and observe MPPT algorithm implementation techniques for PV pumping applications," *IEEE Trans. Sustain. Energy*, vol. 3, no. 1, pp. 21–33, Jan. 2012.
- [16] D. Sera, L. Mathe, T. Kerekes, S. V. Spataru, and R. Teodorescu, "On the Perturb-and-Observe and incremental conductance MPPT methods for PV systems," *IEEE J. Photovolt.*, vol. 3, no. 3, pp. 1070–1078, Jul. 2013.
- [17] E. Dallago, A. Liberale, D. Miotti, and G. Venchi, "Direct MPPT algorithm for PV sources with only voltage measurements," *IEEE Trans. Power Electron.*, vol. 30, no. 12, pp. 6742–6750, Dec. 2015.
- [18] J. Ahmed and Z. Salam, "A modified P&O maximum power point tracking method with reduced steady-state oscillation and improved tracking efficiency," *IEEE Trans. Sustain. Energy*, vol. 7, no. 4, pp. 1506–1515, Oct. 2016.
- [19] M. Killi and S. Samanta, "Modified perturb and observe MPPT Algorithm for drift avoidance in photovoltaic systems," *IEEE Trans. Ind. Electron.*, vol. 62, no. 9, pp. 5549–5559, Sep. 2015.
- [20] G. Escobar, S. Pettersson, C. N. M. Ho, and R. Rico-Camacho, "Multisampling maximum power point tracker (MS-MPPT) to compensate irradiance and temperature changes," *IEEE Trans. Sustain. Energy*, vol. 8, no. 3, pp. 1096–1105, Jul. 2017.
- [21] L. M. Elobaid, A. K. Abdelsalam, and E. E. Zakzouk, "Artificial neural network-based photovoltaic maximum power point tracking techniques: A survey," *IET Renewable Power Gener.*, vol. 9, no. 8, pp. 1043–1063, Nov. 2015.
- [22] S. Mohanty, B. Subudhi, and P. K. Ray, "A grey wolf-assisted perturb & observe MPPT algorithm for a PV system," *IEEE Trans. Energy Convers.*, vol. 32, no. 1, pp. 340–347, Mar. 2017.
- [23] H. Li, D. Yang, W. Su, J. Lu, and X. Yu, "An overall distribution particle swarm optimization MPPT algorithm for photovoltaic system under partial shading," *IEEE Trans. Ind. Electron.*, vol. 66, no. 1, pp. 265–275, Jan. 2019.
- [24] A. A. S. Mohamed, A. Berzoy, and O. A. Mohammed, "Design and hardware implementation of FL-MPPT control of PV systems based on GA and small-signal analysis," *IEEE Trans. Sustain. Energy*, vol. 8, no. 1, pp. 279–290, Jan. 2017.
- [25] D. F. Teshome, C. H. Lee, Y. W. Lin, and K. L. Lian, "A modified firefly algorithm for photovoltaic maximum power point tracking control under partial shading," *IEEE Trans. Emerg. Sel. Top. Power Electron.*, vol. 5, no. 2, pp. 661–671, Jun. 2017.
- [26] K. S. Tey and S. Mekhilef, "A fast-converging MPPT technique for photovoltaic system under fast varying solar irradiation and load resistance," *IEEE Trans. Ind. Informat.*, vol. 11, no. 1, pp. 176–186, Dec. 2014.
- [27] R. C. Dorf and R. H. Bishop, *Modern Control Systems*, 12th ed., Upper Saddle River, NJ, USA: Pearson, Education, 2011, pp. 583–585.
- [28] N. Kumar, I. Hussain, B. Singh, and B. K. Panigrahi, "Maximum power peak detection of partially shaded PV panel by using intelligent monkey king evolution algorithm," *IEEE Trans. Ind. Appl.*, vol. 53, no. 6, pp. 5734–5743, Jul. 2017.



**Vibhu Jatley** received the Ph.D. degree in electrical engineering from the College of Technology, G. B. Pant University, Pantnagar, India, in 2017. Since July 2019, he has been a Postdoctoral Fellow with MCAST Energy Research Group, MCAST, Paola, Malta. He has more than four years of teaching experience, during which he has also worked under United Nations Development Programme, Ethiopia. His research interests include control in photovoltaic systems, control in power electronics, and grid-connected photovoltaic systems.



**Somesh Bhattacharya** (Member, IEEE) received the Ph.D. degree from the Indian Institute of Technology Delhi, New Delhi, India in 2018. He is currently a Postdoctoral Fellow with the MCAST Energy Research Group, MCAST, Paola, Malta. He was briefly employed as an Assistant Professor with Electrical Engineering Department, Siksha 'O' Anusandhan University, Bhubaneswar, India. His research interests include operation and control of microgrids and stability assessment of active distribution networks with high renewable penetration.



**Brian Azzopardi** (Senior Member, IEEE) received the B.Eng. degree from The University of Malta, Msida, Malta, in 2002 and the Ph.D. degree from The University of Manchester, Manchester, U.K., in 2011. He is currently a Senior Academic with the Malta College of Arts, Science, and Technology, Paola, Malta and leads the Energy Research Group, and Visiting Senior Lecturer with The University of Malta. His research interests include photovoltaics and electric mobility network integration and future urban low-carbon society.



**Antoine Montgareuil** graduated from the French Ecole des Mines de Paris. Eng., Paris, France. During his first year of work, he was a Teacher. After the master's in computer science, he joined National Institute for Research in computer science and automation, Le Chesnay-Rocquencourt, France and a startup in Artificial Intelligence. Before joining the Solar Group in 1998, he joined CEA Cadarache, Saint-Paul-lez-Durance, France, where he worked on several matters: management systems and knowledge engineering. His research interests include the performance of photovoltaics, the measurement and the modeling of solar resource, including irradiance prediction with satellite data, and the sizing of energy storage systems, energy systems for insular territories, with high penetration of intermittent energy and of electric mobility.

of photovoltaics, the measurement and the modeling of solar resource, including irradiance prediction with satellite data, and the sizing of energy storage systems, energy systems for insular territories, with high penetration of intermittent energy and of electric mobility.



**Jyoti Joshi** received the B.Tech. degree in electrical and electronics engineering from Uttarakhand Technical University, Dehradun, India, and the M.Tech. degree from Uttar Pradesh Technical University, Lucknow, India, in 2011 and 2015, respectively. She is currently working toward the Ph.D. degree in electrical engineering from the G. B. Pant University of Agriculture and Technology, Pantnagar, India. She has more than seven years of teaching experience during which she was also a Lecturer under United Nations Development Programme, Addis Ababa,

Ethiopia. Her research interests include current controllers in grid-connected photovoltaic systems, fault ride through in grid-connected photovoltaic systems, and flexible power point tracking in photovoltaic systems.



**Sudha Arora** (Member, IEEE) was born in Salia, UP, India, on July 1, 1964. She graduated from the College of Technology, G. B. Pant University of Agriculture and Technology, Pantnagar, India, the M.E. degree in electrical engineering (System Engineering Operations Research) from the Indian Institute of Technology Roorkee, Roorkee, India, and the Ph.D. degree from the Indian Institute of Technology Kanpur, Kanpur, India, in 1987, 1991, and 2006, respectively.

She is currently a Professor and the Head, the Department of Electrical Engineering, College of Technology, Pantnagar, G. B. Pant University of Agriculture and Technology. She was with Lohia Packaging Machines, Kanpur, India. In 1991, she joined as an Assistant Professor with the Department of Electrical Engineering, College of Technology, Pantnagar, where she became an Associate Professor in 2003 and a Professor in 2008. She has one patent application published in patent office journal, guided three Ph.D. thesis and 12 M.Tech. thesis. Her research interests include solar PV, power electronics, and control system.

She is a Fellow of the Institution of Engineers. She is also a Life Member of the Indian Society for Technical Education and Semiconductor Society, India. She has been the Coordinator of the Center of Excellence, Pantnagar, India.